

Article

# Characterization of the Novel Ene Reductase Ppo-Er1 from *Paenibacillus Polymyxa*

David Aregger, Christin Peters  and Rebecca M. Buller \* 

Competence Center for Biocatalysis, Institute of Chemistry and Biotechnology, Department of Life Sciences and Facility Management, Zurich University of Applied Sciences, Einsiedlerstrasse 31, 8820 Waedenswil, Switzerland; David.Aregger@zhaw.ch (D.A.); Christin.peters@zhaw.ch (C.P.)

\* Correspondence: rebecca.buller@zhaw.ch; Tel.: +41-58-934-5438

Received: 31 January 2020; Accepted: 14 February 2020; Published: 19 February 2020



**Abstract:** Ene reductases enable the asymmetric hydrogenation of activated alkenes allowing the manufacture of valuable chiral products. The enzymes complement existing metal- and organocatalytic approaches for the stereoselective reduction of activated C=C double bonds, and efforts to expand the biocatalytic toolbox with additional ene reductases are of high academic and industrial interest. Here, we present the characterization of a novel ene reductase from *Paenibacillus polymyxa*, named Ppo-Er1, belonging to the recently identified subgroup III of the old yellow enzyme family. The determination of substrate scope, solvent stability, temperature, and pH range of Ppo-Er1 is one of the first examples of a detailed biophysical characterization of a subgroup III enzyme. Notably, Ppo-Er1 possesses a wide temperature optimum ( $T_{\text{opt}}$ : 20–45 °C) and retains high conversion rates of at least 70% even at 10 °C reaction temperature making it an interesting biocatalyst for the conversion of temperature-labile substrates. When assaying a set of different organic solvents to determine Ppo-Er1's solvent tolerance, the ene reductase exhibited good performance in up to 40% cyclohexane as well as 20 vol% DMSO and ethanol. In summary, Ppo-Er1 exhibited activity for thirteen out of the nineteen investigated compounds, for ten of which Michaelis–Menten kinetics could be determined. The enzyme exhibited the highest specificity constant for maleimide with a  $k_{\text{cat}}/K_{\text{M}}$  value of 287  $\text{mM}^{-1} \text{s}^{-1}$ . In addition, Ppo-Er1 proved to be highly enantioselective for selected substrates with measured enantiomeric excess values of 92% or higher for 2-methyl-2-cyclohexenone, citral, and carvone.

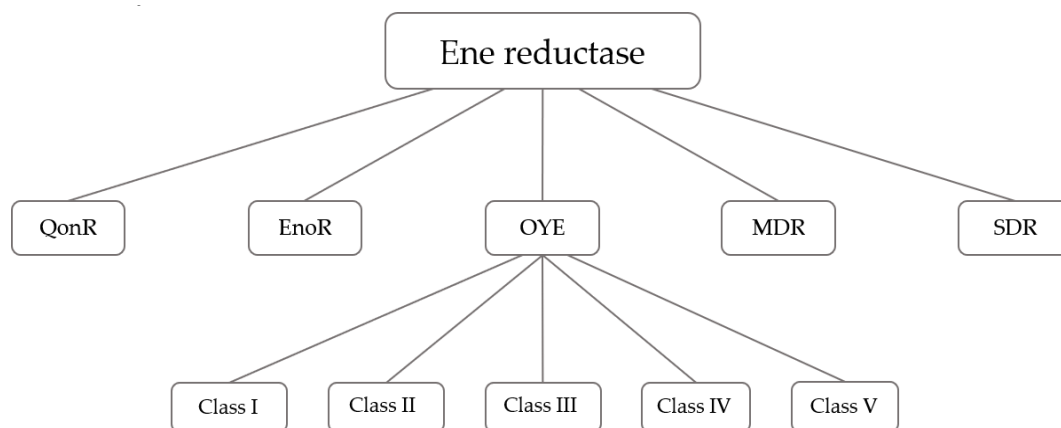
**Keywords:** biocatalysis; ene reductase; enzyme sourcing; old yellow enzyme; solvent stability

## 1. Introduction

Many bioactive molecules contain at least one chiral center rendering the development of effective asymmetric synthesis methods essential for the chemical industry. Besides the well-established metal- and organocatalytic approaches [1], biocatalytic strategies offer an interesting alternative to install chirality into small molecules. To date, industrial biocatalysis has mastered a range of enzyme families including ketoreductases [2], transaminases [3], and imine reductases [4]. Looking forward, the increasing power of genomic mining and enzyme engineering will allow industrial access to even more enzyme families leading to an expansion of the available biocatalytic toolbox [5].

The families of enzymes collectively known as ene reductases (ERs) catalyze the stereoselective trans- and, more rarely, cis-hydrogenation of activated alkenes [6–9]. Thus, ene reductases offer a valuable access route to asymmetric compounds, which is complementary to the chemical cis-hydrogenation catalyzed by chiral rhodium or ruthenium phosphine catalysts [10,11]. Today, ene reductases are classified into five enzyme groups, which differ in structure, reaction mechanism, substrate spectrum, and stereoselectivity (Figure 1) [12]. While enoate reductases, medium- and short-chain dehydrogenases/reductases (MDR and SDR), as well as the recently discovered quinone

reductase-like ene reductases [13], are currently being investigated in terms of their industrial potential [14], enzymes stemming from the old yellow enzyme (OYE) family are established members of the biocatalytic toolbox and are the best characterized and most extensively employed ene reductases today [6].



**Figure 1.** Overview of the classification within the ene reductase family [15]. QnoR (NADPH-dependent quinone reductase like ene-reductases), EnoR (enoate reductase), OYE (old yellow enzyme), MDR (medium-chain dehydrogenase/reductase), and SDR (short-chain dehydrogenase/reductase); Class I (classical OYE); Class II (thermophilic-like OYE) and Class V (fungal OYE).

Isolated in 1932 by Warburg and Christian from bottom-fermented brewer's yeast (*Saccharomyces pastorianus*), the first such ene reductase was named "yellow enzyme" [16]. After the discovery of several additional members belonging to the same enzyme family the "yellow enzyme" was renamed to "old yellow enzyme" (OYE1) [17]. OYEs preferentially accept  $\alpha,\beta$ -unsaturated ketones, aldehydes, nitroalkenes, and some carboxylic acids as substrates [7]. In the last decade, the catalytic mechanism of OYEs has been exhaustively investigated and its general principle is well understood: The enzymes follow a bi-bi ping-pong mechanism, which can be divided into a reductive and an oxidative half reaction [18]. In the reductive half-reaction, flavin mononucleotide (FMN) is reduced through hydride transfer from NAD(P)H, whereas in the oxidative half reaction a hydride is transferred from the reduced flavin to the  $C_\beta$  of the activated alkene. The missing proton for the  $C_\alpha$  is transferred via a tyrosine residue from the opposite site [18,19], ultimately leading to an anti-addition hydrogenation.

The catalytic machinery of OYE enzymes is supported by a typical ( $\alpha,\beta$ ) 8-barrel (TIM-barrel) fold with additional secondary structural elements present (e.g., four  $\beta$ -strands and five  $\alpha$ -helices in OYE1 [20]; six  $\beta$ -strands and two  $\alpha$ -helices in 12-oxophytodienoate reductase OPR [18]). The folded domain is known to occur in different oligomeric states, such as monomers (PETN reductase) [21], dimers (OYE1) [20], tetramers (dimers of dimers such as YqjM [22] or TOYE [23]), octamers, and dodecamers [23]. The oligomerization state is described to be often governed by the position and amino acid composition of surface loops [7]. In addition, the constitution of the loops can have an influence on thermostability [23].

Notably, amino acid sequence alignments of OYE homologs show high conservation in specific regions of the proteins, such as residues involved in catalysis, FMN, and substrate binding [7,15,23]. To account for these differences in sequence and the resulting structural features, the old yellow enzyme family can be further divided into five subclasses [15]. While enzyme members of the subclass I, also termed "classical" old yellow enzymes, and class II, introduced by Scrutton's group in 2010 and dubbed "thermophilic-like" [23], have been well explored [7,14], the recently described class III–V are less well investigated [15,24].

Synthetic applications of ene reductases are manifold and range from the preparation of profens [25–27] and chiral amino acids [28–30] to the synthesis of chiral phosphonates [31] and

nitroalkanes [32], precursors in the synthesis of pharmaceutically active ingredients. To further promote an off-the-shelf synthetic use of ene reductases, which can reduce the time and cost of the implementation of a biocatalytic step into a process significantly, we set out to expand the available biocatalytic toolbox [15]. In this context, not only the discovery and engineering of novel ene reductases is of great utility [33], but also a careful characterization of the new biocatalysts is needed as it may lead to the construction of a more targeted enzyme library associated with reduced screening time and costs.

Herein, we showcase the detailed characterization of Ppo-Er1 from *Paenibacillus polymyxa*, an OYE subclass III enzyme, and highlight the enzyme's substrate scope, kinetic parameters, solvent tolerance, as well as pH and temperature profile. The data presented may facilitate future screening and engineering studies and, in selected cases, thus, lead to the faster adoption of an ene reductase in chemical process development.

## 2. Results and Discussion

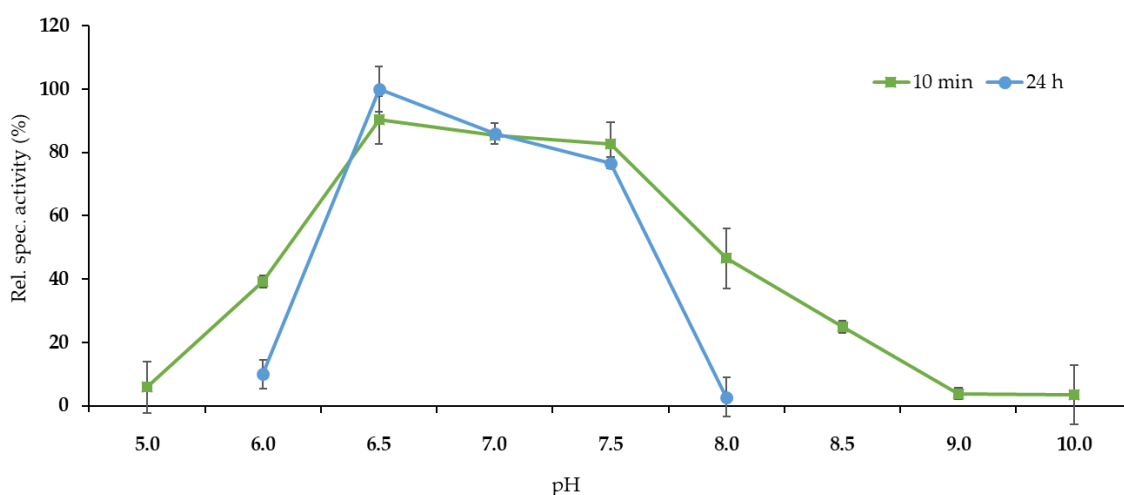
The enzyme Ppo-Er1 from *P. polymyxa* was discovered during the screening of 19 bacterial wild-type strains from the Culture Collection of Switzerland, as previously described [15]. Ppo-Er1 (41.3 kDa) is characterized by a substantial sequence similarity with the old yellow enzyme YqiG from *Bacillus subtilis* (50%) [34], Bac-OYE2 from *Bacillus* sp. (50%) [35], Lla-Er from *Lactococcus lactis* (39%) [15], and LacER from *Lactobacillus paracasei* (47%) [36], all of which belong to the subclass III of the OYE family. In detail, Ppo-Er1 contains a specific combination of motifs known from the classical and thermophilic-like groups that has been found to be characteristic for class III enzymes [15]: Gln104 and Arg228 predicted to interact with the pyrimidine ring of FMN [22], His 171, and Asn 175 proposed to interact with N1 and N3 of FMN [22,37]; Thr30 suggested to interact with isoalloxazine ring O4 of FMN [38]; and Met29, Leu324, and Arg321, which presumably interact with the dimethyl benzene moiety of FMN. As expected, subclass III old yellow enzyme Ppo-Er1 is thus phylogenetically positioned between classical and thermophilic-like OYEs.

### 2.1. Expression and Characterization of Ppo-Er1

The ready-to-use plasmid consisting of pET-28b(+) vector and the Ppo-Er1 sequence was assembled by Twist Bioscience and a C-terminal His<sub>6</sub> tag for protein purification by affinity chromatography was included. The soluble recombinant expression of Ppo-Er1 in *Escherichia coli* BL21 (DE3) was achieved in terrific broth (TB) medium at 25 °C. Ppo-Er1 was purified by affinity chromatography using Ni-NTA resin (Figure S1) and the cofactor FMN was reconstituted before further analysis. FMN reconstitution (100 µM) proved necessary to obtain a fully active enzyme as without this step the enzyme preparation only exhibited 8% (0.05 U/mg for cyclohexanone) of the expected activity (0.61 U/mg for cyclohexanone). This effect was also described for the OYEs LacER [36] and Lla-Er [15]. In the case of LacER, for example, the addition of FMN after purification by DEAE ion exchange chromatography increased the activity by a factor of 92 from 0.0018 to 0.168 U/mg for the substrate *trans*-2-hexen-1-al. This observation suggests that—similar to other known OYEs—the binding affinity of Ppo-Er1 to FMN under purification conditions is low, a fact that has to be kept in mind for any following activity analysis. The storage stability of the purified Ppo-Er1 proved to be very good, boding well for the enzyme's incorporation in potential enzyme screens: At −20 °C and in the presence of 20% glycerol, the enzyme did not lose any activity even when stored for an extended period of time (one week), whereas an activity drop of approximately 20% was observed after incubation for 10 days at 4 °C (no additives). In contrast to a number of reported OYEs [15,39], we found that NADPH and NADH are equally preferred physiological cofactors of Ppo-ER1 (Figure S14) allowing for maximum flexibility in the choice of recycling system during process development. Both, the coupled-enzyme approach [40] or the use of alternative hydride sources [41,42] will thus be conceivable options to avoid having to add stoichiometric amounts of the coenzymes.

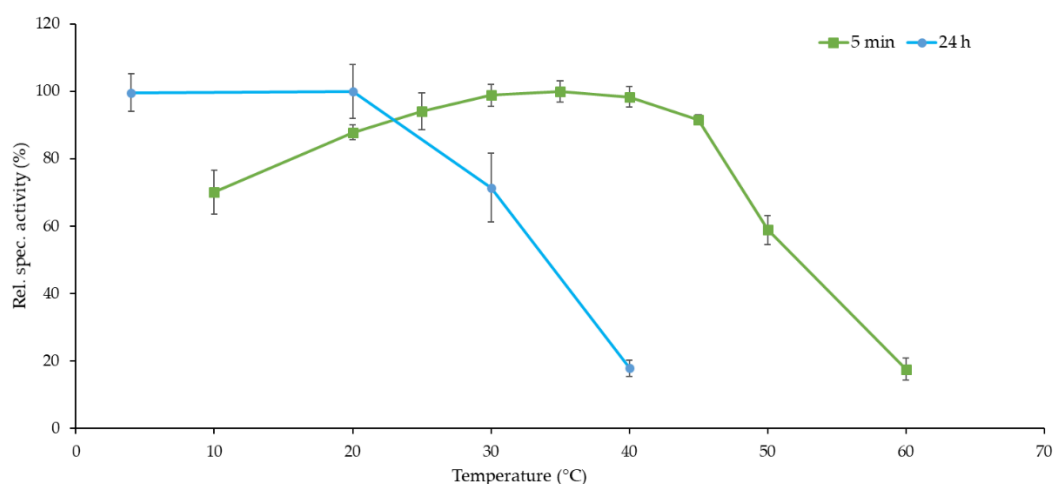
The oligomeric state of Ppo-Er1 was determined via gel filtration by correlation with a commercial gel filtration standard containing proteins of specific size. Based on this comparison, Ppo-Er1 mostly occurs as a monomer (Figure S2) as do for example PETN from *Enterobacter cloacae* [21] and RmER from *Ralstonia metallidurans* [43], both thermophilic-like ene reductases.

Further relevant parameters for application such as optimum pH, optimum temperature, and long-term temperature stability were determined using the substrate cyclohexenone. The pH profile of Ppo-Er1 was measured in Davies buffer covering pH 5 to pH 10 [44], in which the enzyme reached about 50% of the activity observed in 50 mM phosphate buffer (Figure S3). The pH profile was found to be bell-shaped, exhibiting a narrow optimum at pH 6.5–7.5 (Figure 2). Beyond this range, enzyme activity decreases rapidly, especially when the enzyme was pre-incubated for a longer time period (24 h) in the measurement buffers (Figure 2). In the case of other characterized class III OYEs such as LacER [36] and YqiG [15,34], a similar pH profile was determined albeit with a wider pH working range as indicated by the reported optimum activities in the range of  $\text{pH}_{\text{opt}}$  8–9 and  $\text{pH}_{\text{opt}}$  6–9, respectively. Notably, OYE enzymes belonging to other subclasses exhibit similar pH profiles as reported for Ppo-Er1, e.g., the “classical” XenB [45] and NemA [45] with a  $\text{pH}_{\text{opt}}$  of 6–7.5, the “thermophilic-like” YqjM [46] and Chr-OYE3 [47] with a  $\text{pH}_{\text{opt}}$  of 6–8, and the class IV enzyme Ppo-Er3 [15] with a  $\text{pH}_{\text{opt}}$  of 7–8.5.



**Figure 2.** pH profile of Ppo-Er1 measured between pH 5 and pH 10 in Davies buffer [44]. The enzyme was preincubated at 25 °C in the respective measurement buffer solution for 10 min and 24 h, respectively, to determine the stability and activity of Ppo-Er1 in dependence of pH. Relative specific activity corresponds 100% to an activity of 0.41 U/mg for cyclohexenone. The error bars show the standard deviation of triplicates.

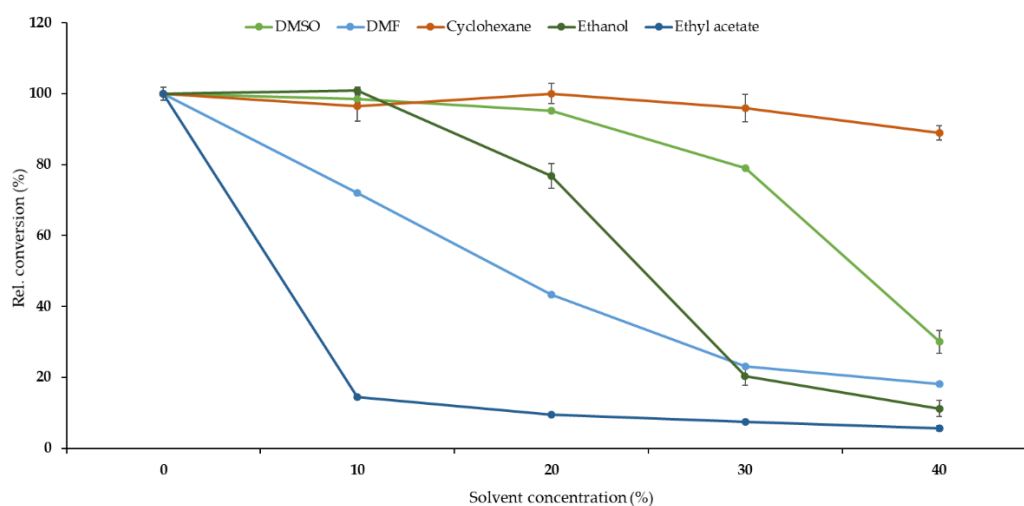
In terms of thermal robustness, Ppo-Er1 possesses interesting long-term stability. After 24 h incubation at 20 °C, enzyme activity toward cyclohexenone remained virtually unchanged, whereas residual activity of approximately 70% was detected after an equally long incubation time at 30 °C. Furthermore, short-term exposure of Ppo-Er1 to 45 °C led to only a marginal loss in activity (<10%) allowing the enzyme to be used for applications that require higher temperatures (Figure 3). These results are in line with data obtained for other class III and IV enzymes such as YqiG and Ppo-Er3, which have reported  $T_{\text{opt}}$  values of 25–40 °C [15,34]. Strikingly, Ppo-Er1 retained a relative specific activity of >70% at temperatures as low as 10 °C making the enzyme an interesting candidate to be used for the transformation of thermolabile substrates such as aldehydes (Figure 3). Overall, our Ppo-Er1 data confirm that the temperature profile of class III enzymes resembles those of their mesophilic counterparts of class I, for example NemA [45] with a reported  $T_{\text{opt}}$  of 30–50 °C and OYE2p [48] with a  $T_{\text{opt}}$  of 25–40 °C. Finally, we employed the ThermoFAD technique to determine the melting temperature of Ppo-Er1 and found that the ene reductase unfolds at  $T_m = 46.5 \pm 1$  °C (Figure S15).



**Figure 3.** The temperature profile and the temperature stability of Ppo-Er1. For the temperature profile Ppo-Er1 was incubated for 5 min at different temperatures (10–60 °C) and directly measured for the conversion of substrate cyclohexenone (1 mM). For the temperature stability measurement, Ppo-Er1 was incubated at four different temperatures (4–40 °C) and measured after 24 h at 25 °C. The error bars show the standard deviation of triplicates. Relative specific activity corresponds 100% to an activity of 0.52 U/mg for cyclohexenone.

The use of cosolvents is often a “must” in biocatalytic processes due to the presence of high concentrations of various organic substrates. Consequently, in many instances the solvent stability of enzymes needs to be optimized by enzyme engineering to generate catalysts that are compatible with the process conditions [49]. To verify the stability of Ppo-Er1 in the presence of a set of typical solvents, we thus determined the enzymatic activity over a concentration range of 10–40% of DMSO, DMF, cyclohexane, ethanol, and ethyl acetate. The enzyme performed best in cyclohexane (assayed substrate: 1 mM hexenal), which did not cause a significant loss in activity even when supplemented to a final volume of up to 40% in the assay. Alternatively, DMSO could be considered as a viable cosolvent for Ppo-Er1 as the enzyme was virtually unaffected up to a concentration of 20% *v/v*. Even at a concentration of 30% *v/v* DMSO, Ppo-Er1 retained a relative activity of approximately 80% (assay substrate: 1 mM cyclohexenone). The solvent ethanol was shown to also be a suitable choice for this enzyme, as it was tolerated well up to a concentration of 10% *v/v*. DMF or ethyl acetate, however, should not be used in combination with Ppo-Er1 as their presence was found to be detrimental for enzymatic activity. Already at a concentration of 10% *v/v* activity drops of 30% and 85% were observed, respectively (Figure 4).

In comparison to most known old yellow enzymes, Ppo-Er1 exhibits similar solvent resistance: The thermophilic-like OYE YqjM [46] has been reported to remain active in an analogous concentration range of DMSO, DMF, and ethyl acetate as Ppo-Er1. However, an ethanol concentration of 10% *v/v* led to a strong reduction of the half-life of YqjM, which we did not observe in the case of Ppo-Er1. TOYE [23], another thermophilic-like OYE, was reported to exhibit a 50% loss of activity at an ethanol concentration of 45% corresponding to a higher stability toward this solvent compared to Ppo-Er1, whereas the classical PETNR [50] already lost 50% activity in the presence of an ethanol concentration of 20% *v/v*. In this context, it should be noted that organic-solvent-tolerant ene reductases have also been reported: FOYE1, originating from an acidophilic iron oxidizer, was shown to perform well in many solvent systems with up to 20% *v/v* solvents (ethanol, methanol, acetone, isopropanol, DMSO, THF) clearly outperforming all abovementioned ene reductases in terms of solvent stability [51].



**Figure 4.** Overview of the solvent stability of Ppo-Er1 in DMSO (dimethyl sulfoxide), DMF (dimethyl formamide), cyclohexane, ethanol, and ethyl acetate in a concentration range of 10%–40% *v/v*. The standard enzyme assay was performed while the concentration of solvents was varied (substrate for cyclohexane: 1 mM hexenal, all other solvents: 1 mM cyclohexenone). Data are shown as values relative to an enzyme assay without cosolvent in which 100% relative conversion corresponds to the production of 0.84 mM cyclohexanone or 0.49 mM hexanal, respectively. The error bars show the standard deviation of triplicates, except for the 30% *v/v* cyclohexane point for which only two measurements were available.

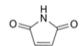
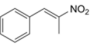
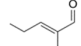
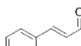

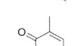
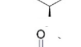

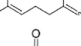
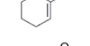
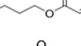
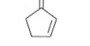
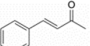
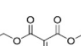
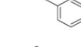
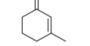
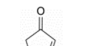
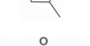
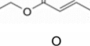
## 2.2. Substrate Scope, Determination of Michaelis–Menten Parameters, and Stereoselectivity

To determine the substrate profile of Ppo-Er1, the enzyme was tested for the conversion of nineteen structurally diverse aliphatic and cyclic alkenes bearing ketone, aldehyde, nitro, carboxylic acid, or ester moieties as electron-withdrawing groups. For thirteen substrates, product formation by Ppo-Er1 could be detected. Cyclohexenone, hexenal, 2-methyl-2-pentenal, 4-phenyl-3-buten-2-one, cinnamic aldehyde, maleimide, and carvone (at 5 mM concentration) were converted especially well, and >99% conversion was obtained within 4 h (Table 1). Substrates not accepted by Ppo-Er1 included  $\alpha,\beta$ -unsaturated carboxylic acids such as butenic acid, cinnamic acid, and citraconic acid as well as the ketones 3-methyl-2-cyclohexenone and 3-methyl-2-cyclopentenone, which are characterized by an additional methyl group in the  $\beta$ -position. The  $\alpha,\beta$ -unsaturated ester ethyl crotonate was also not converted.

Based on the obtained data, it can be concluded that the overall substrate profile of Ppo-Er1 resembles that of other subclass III enzymes such as YqiG [15,34] and Lla-Er [15]. For example, 5 mM of cinnamic aldehyde and cyclohexenone are also well converted by Lla-Er [15] ( $65\% \pm 4.2\%$  and  $23\% \pm 3.1\%$ ) and YqiG [15] ( $58\% \pm 2.4\%$  and  $55\% \pm 6.1\%$ ) after 1 h at 30 °C. Notably, however, marked differences in substrate acceptance by class III enzymes occur for some of the investigated substrates highlighting the importance of an in-depth substrate profiling: Whereas carvone and maleimide are very well converted by Ppo-Er1 (both: >99%), Lla-Er, for example, accepts this compound only poorly (carvone:  $2.6\% \pm 0.1\%$ , maleimide: not converted) [15]. Diethylbenzylidenemalonate conversion by YqiG [15,34] ( $11\% \pm 1.3\%$ ), on the other hand, significantly exceeded the detected product formations achieved by Lla-Er (<1%) [15] and Ppo-Er1 (1.2%). Moreover, 3-methyl-2-cyclopentenone, which is not converted by Ppo-Er1, Lla-Er [15], and YqiG [15,34], has been shown to be accepted by LacER [36]. Generally, we noted that Ppo-Er1 has a restricted substrate acceptance for cyclic  $\beta$ -methylated substrates such as 3-methyl-2-cyclohexenone and 3-methyl-2-cyclopentenone, which possibly results from a difficulty in accepting substituents at the  $C_\beta$  position of cyclic compounds in the active site in analogy to other class II, III, and IV enzymes [15,39]. In addition, carboxylic acids

and esters seem to be non-optimal alkene activating groups for this enzyme as conversion of the corresponding substrates was low or not detectable.

**Table 1.** Conversion, steady state kinetics,<sup>(a)</sup> and enantiomeric excess (ee) of various substrates converted with purified enzymes as determined after 4 h at 20 °C (n.d.: not detected; n.s.: not soluble). The given uncertainties show the standard deviation of triplicates.

Substrate		Conversion	ee	$k_{cat}/K_m$	$K_m$	$k_{cat}$
Name	Structure	(%)	(%)	( $\text{mM}^{-1} \text{s}^{-1}$ )	(mM)	( $\text{s}^{-1}$ )
Maleimide		$\geq 99 \pm 3.7$		$287.8 \pm 0.12$	$0.10 \pm 0.01$	$28.78 \pm 0.62$
<i>trans</i> - $\beta$ -Methyl- $\beta$ -nitrostyrene		$81 \pm 1.0$		$41.4 \pm 0.23$	$0.12 \pm 0.03$	$4.97 \pm 0.36$
2-Methyl-2-pentenal		$\geq 99 \pm 7.4$	(S) 63	$15.3 \pm 0.09$	$0.41 \pm 0.04$	$6.27 \pm 0.11$
Cinnamaldehyde		$\geq 99 \pm 1.5$		$14.6 \pm 0.14$	$0.36 \pm 0.05$	$5.27 \pm 0.18$
Hexenal		$\geq 99 \pm 3.4$		$3.3 \pm 0.10$	$2.22 \pm 0.21$	$7.42 \pm 0.01$
Carvone		$\geq 99 \pm 2.1$	(R) 98	$0.5 \pm 0.16$	$4.35 \pm 0.69$	$2.20 \pm 0.08$
Cyclohexenone		$\geq 99 \pm 0.5$		$0.4 \pm 0.08$	$13.42 \pm 1.0$	$5.25 \pm 0.1$
Citral		$29 \pm 1.4$	(S) 94	$0.2 \pm 0.93$	$1.12 \pm 1.0$	$0.17 \pm 0.04$
2-Methyl-2-cyclohexenone		$76.2 \pm 0.4$	(R) 92	$0.1 \pm 0.23$	$14.93 \pm 3.3$	$1.30 \pm 0.08$
Cyclopentenone		$59 \pm 1.7$		$0.03 \pm 0.17$	$57.24 \pm 9.4$	$1.75 \pm 0.16$
4-Phenyl-3-buten-2-one		$\geq 99 \pm 1.0$			n.s.	
Butylacrylate		$22 \pm 6.5$				
Diethyl benzyldienemalonate		$1.2 \pm 0.0$				
3-Methyl-2-cyclohexenone		n.d.				
3-Methyl-2-cyclopentenone		n.d.				
Etylcrotonate		n.d.				
Butenoic acid		n.d.				
Cinnamic acid		n.d.				
Citraconic acid		n.d.				

<sup>(a)</sup> Reactions (1 mL) were performed in potassium phosphate buffer (50 mM, pH 7.0) containing NADPH (175  $\mu\text{M}$ ) and substrate (20  $\mu\text{M}$ –80 mM), depending on substrate, Ppo-Er1 (0.61  $\mu\text{M}$ ), and DMSO to solubilize the substrates. The reactions were followed continuously by monitoring NADPH oxidation at 340 nm for 90 sec at 25 °C.

To complement the substrate acceptance profile, Michaelis–Menten parameters of Ppo-Er1 for ten diverse substrates were determined (Table 1, Figures S4–S13). Within the tested substrate range, Ppo-Er1 showed the highest catalytic efficiency for maleimide ( $k_{cat}/K_m = 287 \text{ mM}^{-1} \text{ s}^{-1}$ ) followed by *trans*- $\beta$ -methyl- $\beta$ -nitrostyrene ( $k_{cat}/K_m = 41 \text{ mM}^{-1} \text{ s}^{-1}$ ). In combination with the conversion data, the

measured kinetic parameters (Table 1) indicate a general preference for alkenes carrying a phenyl substituent at the C<sub>β</sub> position of the substrates. Overall, Ppo-Er1's specific activity for other typical ene reductase substrates such as carvone ( $k_{\text{cat}}/K_m = 0.5 \text{ mM}^{-1} \text{ s}^{-1}$ ) and cyclohexanone ( $k_{\text{cat}}/K_m = 0.4 \text{ mM}^{-1} \text{ s}^{-1}$ ) was found to be in a similar range as those described for other well-known OYEs such as the classical PETNR (carvone:  $k_{\text{cat}}/K_m = 2 \text{ mM}^{-1} \text{ s}^{-1}$ ; cyclohexanone:  $k_{\text{cat}}/K_m = 5 \text{ mM}^{-1} \text{ s}^{-1}$ ) [50] and the thermophilic-like YqjM (cyclohexanone:  $k_{\text{cat}}/K_m = 6.4 \text{ mM}^{-1} \text{ s}^{-1}$ ) [46] (Table 2). Maleimide, however, is better converted by ene reductases from photosynthetic extremophiles such as CtOYE ( $k_{\text{cat}}/K_m = 1940 \text{ mM}^{-1} \text{ s}^{-1}$ ) or GsOYE ( $k_{\text{cat}}/K_m = 399 \text{ mM}^{-1} \text{ s}^{-1}$ ) [52] the thermophilic-like OYERo2 ( $k_{\text{cat}}/K_m = 10,800 \text{ mM}^{-1} \text{ s}^{-1}$ ) [53] or the class III OYE YqiG ( $k_{\text{cat}}/K_m = 800 \text{ mM}^{-1} \text{ s}^{-1}$ ) (Table 2).

**Table 2.** Comparison of the catalytic efficiencies ( $\text{mM}^{-1} \text{ s}^{-1}$ ) of a range of known old yellow enzymes (OYEs) (YqiG [34], PETNR [50], YqjM [46], TOYE [23], DrER [43], RmER [43], and OYERo2 [53]) from class I–III.

Substrate	Class I			Class II		Class III		
	PETNR	YqjM	TOYE	DrER	RmER	OYERo2	Ppo-Er1	YqiG
Cyclohexenone	5	6.4	0.5	2.1	0.7		0.4	22
2-Methyl-cyclohexenone	4	1.0					0.1	
Cyclopentenone	<0.5	1.9	0.6				0.03	
Hexenal		0.60					3.3	
Citral	9	0.02	0.05				0.2	6.7
2-Methyl-2-pentenal	61		0.14				15.3	18
Cinnamaldehyde	8						14.6	
Carvone	2		1.5				0.5	7.5
Maleimide						10,800	287.8	800
<i>trans</i> -β-Methyl-β-nitrostyrene							41.4	

In addition to determining the steady-state kinetic parameters, we also investigated the stereopreference of Ppo-Er1. Based on our results with four selected substrates, Ppo-Er1 displays a similar stereopreference to other reported OYE class III enzymes (Table 3), preferentially forming the *S*-product when converting 2-methyl-2-pentenal and citral and forming the *R*-product when transforming carvone and 2-methyl-2-cyclohexenone. Notably, the detected ee values of Ppo-Er1 are generally superior to values determined for YqiG and Lla-Er [15] with the only exception being the enantiomeric excess reported for the conversion of carvone by Lla-Er (>99.9% ee). It should be noted, however, that Lla-Er displayed a low conversion of 2.6% of 5 mM substrate after 1 h at 30 °C compared to the >99% conversion of 5 mM substrate by Ppo-Er1 after 4 h at 20 °C.

**Table 3.** The enantiomeric excess of some selected OYEs (YqiG [15], Lla-Er [15], Ppo-Er3 [15], OPR1 [54], OPR3 [54], PETNR [50], YqjM [54], TOYE [23]) from classes I–IV. The values presented for YqjM were measured as a reference for Ppo-Er1 and compared with the literature [54].

Substrate	OPR1	Class I		PETNR	YqjM	Class II		Class III		Class IV
		OPR3				TOYE	Ppo-Er1	YqiG	Lla-ER	Ppo-Er3
2-Methyl-2-pentenal	( <i>R</i> ) 47	( <i>S</i> ) 78			( <i>R</i> ) 20	( <i>S</i> ) 55	( <i>S</i> ) 63	( <i>S</i> ) 33	( <i>S</i> ) 5	( <i>S</i> ) 67
Carvone			( <i>R</i> ) 95		( <i>R</i> ) 82	( <i>R</i> ) 95	( <i>R</i> ) 98	( <i>R</i> ) 89	( <i>R</i> ) >99.9	( <i>R</i> ) 91
2-Methyl-2-cyclohexenone	( <i>R</i> ) 77	( <i>R</i> ) 62			( <i>R</i> ) 81		( <i>R</i> ) 92	( <i>R</i> ) 83	( <i>R</i> ) 11	( <i>R</i> ) 86
Citral	( <i>S</i> ) >95	( <i>S</i> ) >95			( <i>S</i> ) 95	( <i>S</i> ) 91	( <i>S</i> ) 94			

### 3. Materials and Methods

#### 3.1. Materials

All chemicals were purchased from Merck (Darmstadt, Germany), VWR (Hannover, Germany), or Carl Roth (Karlsruhe, Germany). The purchased chemicals were of the highest available purity or of analytical grade and were used without further purification unless otherwise specified. NADPH tetrasodium salt was ordered from Oriental Yeast Co. Ltd. (Tokyo, Japan). The plasmid (pET 28b(+)



incl. Ppo-Er1) was ordered from Twist Bioscience (San Francisco, CA, USA). The HisTrap FF and the HiTrap Desalting columns were ordered from GE Healthcare (Uppsala, Sweden).

### 3.2. Plasmid

Twist Bioscience (San Francisco, CA, USA) cloned the synthetic gene of the codon optimized Ppo-Er1 (Accession Nr: WP\_013369181) with *Nde*I and *Xho*I in the commercial pET28b(+) vector.

### 3.3. Bacterial Strains and Culture Conditions

*E. coli* BL21 (DE3) [*fhuA2 [lon] ompT gal (λ DE3) [dcm] ΔhsdS*] was purchased from New England Biolabs (Beverly, MA, USA). *E. coli* strains were cultured routinely in Lysogeny broth (LB) or TB media and were supplemented with kanamycin (50 μg mL<sup>-1</sup>). Bacterial cultures were incubated in baffled Erlenmeyer flasks in a New Brunswick Innova 42 orbital shaker at 200 rpm and 37 °C. Bacteria on agar plates were incubated in a HERATherm Thermo Scientific incubator under air. All materials and biotransformation media were sterilized by autoclaving at 121 °C for 20 min. Aqueous stock solutions were sterilized by filtration through 0.22 μm syringe filters. Agar plates were prepared with LB medium supplemented by 1.5% (w/v) agar.

### 3.4. Expression

The expression of Ppo-Er1 in *E. coli* BL21 (DE3) was performed by inoculation of TB media (400 mL) supplemented with kanamycin (50 μg mL<sup>-1</sup>) with an overnight culture (4 mL; 1:100). The culture was incubated at 37 °C and 180 rpm until optical density OD<sub>600</sub> = 0.5–0.8 was reached. Afterward expression was induced by the addition of 100 μM IPTG, and incubation was continued at 25 °C for 18 h. Cells were harvested by centrifugation at 4500× *g* for 10 min at 4 °C and either used directly or the pellet was stored by freezing at –20 °C.

### 3.5. Enzyme Purification

The cell disruption was performed by resuspending the pellet from a 400 mL culture in 20 mL buffer (100 mM sodium phosphate buffer pH 7.5, 300 mM NaCl, supplemented by 30 mM imidazole) and a single passage through a French press (2000 psi). The crude extract was separated from the cell debris by centrifugation at 8000× *g* for 45 min. Purification was achieved by affinity chromatography exploiting the C-terminal His-Tag using an automated Äkta purifier system. The crude extract was filtered (0.45 μm) and applied to a pre-equilibrated 5 mL HisTrap FF column. The unbound protein was washed with five column volumes of buffer supplemented with 45 mM imidazole. The elution of Ppo-Er1 was accomplished by a three-column volume of buffer supplemented with 300 mM imidazole. The resulting fractions were collected and analyzed by SDS-PAGE. The fractions with a high content of Ppo-Er1 were pooled and desalted using 50 mM sodium phosphate buffer (pH 7.5) to remove the imidazole. This step was performed employing the Äkta purifier system using three coupled 5 mL HiTrap desalting columns. After the system was equilibrated, the Ppo-Er1-containing sample was applied and fractionated. The protein fractions were analyzed via the integrated online absorption measurement at 280 nm. The protein content of the pooled purified sample was determined by measuring the adsorption with a NanoDrop One (Thermo Fisher Scientific) system and using the molecular weight (41.3 kDa) and extinction coefficient ( $\epsilon_{\lambda = 280 \text{ nm}} = 38'390 \text{ M}^{-1} \text{ cm}^{-1}$ ) of Ppo-Er1 for the calculation. The extinction coefficient was obtained by using the online calculation tool Prot pi [55].

### 3.6. Activity Assay

The activity measurements were recorded spectrophotometrically by observing NADPH consumption at 340 nm for 60–90 s in a 1 mL (1 cm) plastic cuvette in the Lambda 465 (PDA UV/VIS) system from Perkin Elmer. The biocatalytic experiments to obtain the pH and the temperature profile were conducted in sodium phosphate buffer (50 mM, pH 7.5) using 175 μM NADPH, 1 mM

cyclohexenone, and 0.61  $\mu\text{M}$  purified Ppo-Er1. For the determination of the Michaelis–Menten parameters, the substrate concentration was varied in the range of 20  $\mu\text{M}$ –80 mM depending on the substrate while the enzyme concentration was kept constant at 0.61  $\mu\text{M}$ . For the pH profile, Davies buffer [44] was used. All measurements were done in triplicates. Background NADPH consumption was determined in assays in which either the enzyme or the substrate had been eliminated. The substrates were solubilized as 1 M stock in DMSO.

### 3.7. Biocatalysis Reaction

The in vitro biocatalysis reaction were performed by using desalted Ppo-Er1 (with a concentration of 12.1  $\mu\text{M}$ ), 5 mM substrate (1 M stock in DMSO) supplemented with 100  $\mu\text{M}$  NADPH, 10 mM glucose, and 5  $\mu\text{L}$  GDH (20% w/v cell suspension). The reaction volume was adjusted to 1 mL in a glass vial by using sodium phosphate buffer (200 mM, pH 7.0) and incubated for 4 h at 20 °C and 1000 rpm. To determine the solvent stability of Ppo-Er1, the biocatalysis reaction conditions were adapted to include 2.4  $\mu\text{M}$  Ppo-Er1 and 0%–40% v/v solvent (ethanol, ethyl acetate, DMSO, DMF, cyclohexane) in a total reaction volume of 1 mL for 50 min at 20 °C and 1000 rpm. All biocatalysis reactions were done in triplicate, biocatalysis results were verified by control reactions omitting the enzyme.

### 3.8. GC-Analysis

One milliliter biocatalysis reactions were extracted once with 500  $\mu\text{L}$  methyl *tert*-butyl ether (incl. 1 g/L 1-octanol as internal standard). The phase separation was achieved by centrifugation of the biphasic sample, and the organic phase was separated and subjected to GC analysis (Table S1).

### 3.9. Gel Filtration

For the determination of the oligomeric state of Ppo-Er1, the Äkta purifier system employing a HiLoad 16/600 Superdex 75 pg column (GE Healthcare (Uppsala, Sweden)) and sodium phosphate buffer (50 mM, pH 7.5) was used. In a first step, the system was calibrated by using the gel filtration standard from Bio Rad (1.35–670 kDa Prod. no.: #1511901). Then flavin-saturated Ppo-Er1 was applied to system under identical conditions.

### 3.10. Melting Temperature

The unfolding temperature was determined by a *ThermoFAD* assay [56] using Rotor-Gene Q RT-PCR machine. Protein samples (0.5–0.3 mg/mL) in 20  $\mu\text{L}$  sodium phosphate buffer pH 7 were measured using a temperature gradient from 25 to 90 °C, performing fluorescence measurements every 0.5 °C increase after a 10 s delay for signal stabilization. The measurements were performed in triplicates using 470 nm excitation wavelength and 510 nm emission wavelength.

## 4. Conclusions

Ppo-Er1 is a well-expressed, easy to purify, old yellow enzyme belonging to the recently introduced subclass III designation. In terms of cofactor preference, the enzyme accepts NADPH and NADH equally well, whereas pH and optimum temperature resemble those of previously described OYEs. Notably, the enzyme exhibits only slightly reduced performance (>70% conversion of 1 mM cyclohexenone) at lowered temperatures (10 °C) making it a possible candidate for the transformation of labile substrates such as some aldehydes. In addition, the enzyme was shown to have noteworthy stability in the presence of the solvents cyclohexane (up to at least 40% v/v), DMSO, and ethanol (up to 20% v/v).

The substrate profile analysis with a set of 19 representative alkenes allowed the establishment of Ppo-Er1's substrate scope highlighting its acceptance of a variety of linear and cyclic compounds with often excellent transformation efficiencies and exquisite stereoselectivity (e.g., 98% ee for carvone). Complementing this analysis with the determination of steady-state kinetics for ten of the substrates allowed us to conclude that Ppo-Er1 classifies well with other subgroup III old yellow enzymes.

In summary, our in-depth characterization of Ppo-Er1 allows the enlargement of the available panel of ene reductases with a versatile biocatalyst having interesting synthetic properties. Its introduction in the biocatalytic toolbox may further facilitate academic and industrial efforts when screening for biocatalysts capable of asymmetric double bond reduction. Looking forward, Ppo-Er1's performance could be further optimized via enzyme and process engineering.

**Supplementary Materials:** The following are available online at <http://www.mdpi.com/2073-4344/10/2/254/s1>. Figure S1: SDS-PAGE of the different purification steps for the ene reductase Ppo-ER1; Figure S2: Gel filtration of Ppo-ER1; Figure S3: Activity of Ppo-ER1 in the two used buffers; Table S1: Overview of the used GC-methods; Figure S4: Michaelis–Menten kinetic for maleimide; Figure S5: Michaelis–Menten kinetic for trans- $\beta$ -methyl- $\beta$ -nitrostyrene; Figure S6: Michaelis–Menten kinetic for cyclohexanone; Figure S7: Michaelis–Menten kinetic for cinnamaldehyde; Figure S8: Michaelis–Menten kinetic for 2-methyl-2-pentenal; Figure S9: Michaelis–Menten kinetic for carvone; Figure S10: Michaelis–Menten kinetic for citral; Figure S11: Michaelis–Menten kinetic for 2-methyl-2-cyclohexenone; Figure S12: Michaelis–Menten kinetic for cyclopentenone; Figure S13: Michaelis–Menten kinetic for hexenal; Figure S14: Comparison conversion with NADH and NADPH; Figure S15: Melting curve.

**Author Contributions:** Conceptualization: C.P. and R.M.B.; experimental work: D.A.; writing: D.A., C.P., and R.M.B. All authors have read and agreed to the published version of the manuscript.

**Funding:** This research received no external funding.

**Conflicts of Interest:** The authors declare no conflict of interest.

## References

1. List, B.; Yang, J.W. Chemistry. The organic approach to asymmetric catalysis. *Science* **2006**, *313*, 1584–1586. [[CrossRef](#)] [[PubMed](#)]
2. Huffman, M.A.; Fryszkowska, A.; Alvizo, O.; Borra-Garske, M.; Campos, K.R.; Canada, K.A.; Devine, P.N.; Duan, D.; Forstater, J.H.; Grosser, S.T.; et al. Design of an in vitro biocatalytic cascade for the manufacture of islatravir. *Science* **2019**, *366*, 1255–1259. [[CrossRef](#)] [[PubMed](#)]
3. Savile, C.K.; Janey, J.M.; Mundorff, E.C.; Moore, J.C.; Tam, S.; Jarvis, W.R.; Colbeck, J.C.; Krebber, A.; Fleitz, F.J.; Brands, J.; et al. Biocatalytic asymmetric synthesis of chiral amines from ketones applied to sitagliptin manufacture. *Science* **2010**, *329*, 305–309. [[CrossRef](#)] [[PubMed](#)]
4. Schober, M.; MacDermaid, C.; Ollis, A.A.; Chang, S.; Khan, D.; Hosford, J.; Latham, J.; Ihnken, L.A.F.; Brown, M.J.B.; Fuerst, D.; et al. Chiral synthesis of lsd1 inhibitor gsk2879552 enabled by directed evolution of an imine reductase. *Nat. Catal.* **2019**, *2*, 909–915. [[CrossRef](#)]
5. Adams, J.P.; Brown, M.J.B.; Diaz-Rodriguez, A.; Lloyd, R.C.; Roiban, G.D. Biocatalysis: A pharma perspective. *Adv. Synth. Catal.* **2019**, *361*, 2421–2432. [[CrossRef](#)]
6. Toogood, H.S.; Scrutton, N.S. Discovery, characterisation, engineering and applications of ene reductases for industrial biocatalysis. *ACS Catal.* **2019**, *8*, 3532–3549. [[CrossRef](#)]
7. Toogood, H.S.; Gardiner, J.M.; Scrutton, N.S. Biocatalytic reductions and chemical versatility of the old yellow enzyme family of flavoprotein oxidoreductases. *Chemcatchem* **2010**, *2*, 892–914. [[CrossRef](#)]
8. Winkler, C.K.; Faber, K.; Hall, M. Biocatalytic reduction of activated cc-bonds and beyond: Emerging trends. *Curr. Opin. Chem. Biol.* **2018**, *43*, 97–105. [[CrossRef](#)]
9. Shimoda, K.; Ito, D.I.; Izumi, S.; Hirata, T. Novel reductase participation in the syn-addition of hydrogen to the c=c bond of enones in the cultured cells of *Nicotiana tabacum*. *J. Chem. Soc. Perkin Trans.* **1996**, *1*, 355–358. [[CrossRef](#)]
10. Knowles, W.S. Asymmetric hydrogenations (nobel lecture). *Angew. Chem. Int. Ed. Engl.* **2002**, *41*, 1999–2007.
11. Noyori, R. Asymmetric catalysis: Science and opportunities (nobel lecture). *Angew. Chem. Int. Ed.* **2002**, *41*, 2008–2022. [[CrossRef](#)]
12. Knaus, T.; Toogood, H.S.; Scrutton, N.S. Ene-reductases and their applications. In *Green Biocatalysis*; John Wiley & Sons, Inc.: Hoboken, NJ, USA, 2016; pp. 473–488.
13. Steinkellner, G.; Gruber, C.C.; Pavkov-Keller, T.; Binter, A.; Steiner, K.; Winkler, C.; Lyskowski, A.; Schwamberger, O.; Oberer, M.; Schwab, H.; et al. Identification of promiscuous ene-reductase activity by mining structural databases using active site constellations. *Nat. Commun.* **2014**, *5*, 4150. [[CrossRef](#)] [[PubMed](#)]

14. Hecht, K.; Buller, R. Ene-reductases in pharmaceutical chemistry. In *Pharmaceutical Biocatalysis: Chemoenzymatic Synthesis of Active Pharmaceutical Ingredients*; Grunwald, P., Ed.; Jenny Stanford Publishing: Singapore, 2019.
15. Peters, C.; Frasson, D.; Sievers, M.; Buller, R. Novel old yellow enzyme subclasses. *Chembiochem* **2019**, *20*, 1569–1577. [[CrossRef](#)] [[PubMed](#)]
16. Warburg, O.; Christian, W. Ein zweites sauerstoffübertragendes ferment und sein absorptionspektrum. *Naturwissenschaften* **1932**, *20*, 688. [[CrossRef](#)]
17. Haas, E. Isolierung eines neuen gelben ferments. *Biochem. Z* **1938**, *298*, 369–390.
18. Breithaupt, C.; Strassner, J.; Breiting, U.; Huber, R.; Macheroux, P.; Schaller, A.; Clausen, T. X-ray structure of 12-oxophytodienoate reductase 1 provides structural insight into substrate binding and specificity within the family of oye. *Structure* **2001**, *9*, 419–429. [[CrossRef](#)]
19. Kohli, R.M.; Massey, V. The oxidative half-reaction of old yellow enzyme: The role of tyrosine 196. *J. Biol. Chem.* **1998**, *273*, 32763–32770. [[CrossRef](#)]
20. Fox, K.M.; Karplus, P.A. Old yellow enzyme at 2 Å resolution: Overall structure, ligand binding, and comparison with related flavoproteins. *Structure* **1994**, *2*, 1089–1105. [[CrossRef](#)]
21. Barna, T.M.; Khan, H.; Bruce, N.C.; Barsukov, I.; Scrutton, N.S.; Moody, P.C.E. Crystal structure of pentaerythritol tetranitrate reductase: “Flipped” binding geometries for steroid substrates in different redox states of the enzyme. *J. Mol. Biol.* **2001**, *310*, 433–447. [[CrossRef](#)]
22. Kitzing, K.; Fitzpatrick, T.B.; Wilken, C.; Sawa, J.; Bourenkov, G.P.; Macheroux, P.; Clausen, T. The 1.3 Å crystal structure of the flavoprotein yqjm reveals a novel class of old yellow enzymes. *J. Biol. Chem.* **2005**, *280*, 27904–27913. [[CrossRef](#)]
23. Adalbjörnsson, B.V.; Toogood, H.S.; Fryszkowska, A.; Pudney, C.R.; Jowitt, T.A.; Leys, D.; Scrutton, N.S. Biocatalysis with thermostable enzymes: Structure and properties of a thermophilic ‘ene’-reductase related to old yellow enzyme. *ChemBioChem* **2010**, *11*, 197–207. [[CrossRef](#)] [[PubMed](#)]
24. Nizam, S.; Verma, S.; Borah, N.N.; Gazara, R.K.; Verma, P.K. Comprehensive genome-wide analysis reveals different classes of enigmatic old yellow enzyme in fungi. *Sci. Rep.* **2014**, *4*, 4013. [[CrossRef](#)] [[PubMed](#)]
25. Pietruszka, J.; Schölzel, M. Ene reductase-catalysed synthesis of (r)-profen derivatives. *Adv. Synth. Catal.* **2012**, *354*, 751–756. [[CrossRef](#)]
26. Li, Z.N.; Wang, Z.X.; Meng, G.; Lu, H.; Huang, Z.D.; Chen, F.E. Identification of an ene reductase from yeast *Kluyveromyces marxianus* and application in the asymmetric synthesis of (R)-profen esters. *Asian. J. Org. Chem.* **2018**, *7*, 763–769. [[CrossRef](#)]
27. Waller, J.; Toogood, H.S.; Karupiah, V.; Rattray, N.J.W.; Mansell, D.J.; Leys, D.; Gardiner, J.M.; Fryszkowska, A.; Ahmed, S.T.; Bandichhor, R.; et al. Structural insights into the ene-reductase synthesis of profens. *Org. Biomol. Chem.* **2017**, *15*, 4440–4448. [[CrossRef](#)] [[PubMed](#)]
28. Fryszkowska, A.; Fisher, K.; Gardiner, J.M.; Stephens, G.M. A short, chemoenzymatic route to chiral  $\beta$ -aryl- $\gamma$ -amino acids using reductases from anaerobic bacteria. *Org. Biomol. Chem.* **2010**, *8*, 533–535. [[CrossRef](#)] [[PubMed](#)]
29. Winkler, C.K.; Clay, D.; Davies, S.; O’Neill, P.; McDaid, P.; Debarge, S.; Steflik, J.; Karmilowicz, M.; Wong, J.W.; Faber, K. Chemoenzymatic asymmetric synthesis of pregabalin precursors via asymmetric bioreduction of  $\beta$ -cyanoacrylate esters using ene-reductases. *J. Org. Chem.* **2013**, *78*, 1525–1533. [[CrossRef](#)]
30. Winkler, C.K.; Clay, D.; Turrini, N.G.; Lechner, H.; Kroutil, W.; Davies, S.; Debarge, S.; O’Neill, P.; Steflik, J.; Karmilowicz, M.; et al. Nitrile as activating group in the asymmetric bioreduction of beta-cyanoacrylic acids catalyzed by ene-reductases. *Adv. Synth. Catal.* **2014**, *356*, 1878–1882. [[CrossRef](#)]
31. Janicki, I.; Kiełbasiński, P.; Turrini, N.G.; Faber, K.; Hall, M. Asymmetric bioreduction of  $\beta$ -activated vinylphosphonate derivatives using ene-reductases. *Adv. Synth. Catal.* **2017**, *359*, 4190–4196. [[CrossRef](#)]
32. Bertolotti, M.; Brenna, E.; Crotti, M.; Gatti, F.G.; Monti, D.; Parmeggiani, F.; Santangelo, S. Substrate scope evaluation of the enantioselective reduction of  $\beta$ -alkyl- $\beta$ -arylnitroalkenes by old yellow enzymes 1–3 for organic synthesis applications. *ChemCatChem* **2016**, *8*, 577–583. [[CrossRef](#)]
33. Dobrijevic, D.; Benhamou, L.; Aliev, A.E.; Méndez-Sánchez, D.; Dawson, N.; Baud, D.; Tappertzhofen, N.; Moody, T.S.; Orengo, C.A.; Hailes, H.C.; et al. Metagenomic ene-reductases for the bioreduction of sterically challenging enones. *RSC Adv.* **2019**, *9*, 36608–36614. [[CrossRef](#)]
34. Sheng, X.; Yan, M.; Xu, L.; Wei, M. Identification and characterization of a novel old yellow enzyme from *Bacillus subtilis* str.168. *J. Mol. Catal. B Enzym.* **2016**, *130*, 18–24. [[CrossRef](#)]

35. Zhang, H.; Gao, X.; Ren, J.; Feng, J.; Zhang, T.; Wu, Q.; Zhu, D. Enzymatic hydrogenation of diverse activated alkenes. Identification of two bacillus old yellow enzymes with broad substrate profiles. *J. Mol. Catal. B Enzym.* **2014**, *105*, 118–125. [[CrossRef](#)]
36. Gao, X.; Ren, J.; Wu, Q.; Zhu, D. Biochemical characterization and substrate profiling of a new nadh-dependent enoate reductase from *Lactobacillus casei*. *Enzyme Microb. Technol.* **2012**, *51*, 26–34. [[CrossRef](#)] [[PubMed](#)]
37. Brown, B.J.; Deng, Z.; Karplus, P.A.; Massey, V. On the active site of old yellow enzyme: Role of histidine 191 and asparagine 194. *J. Biol. Chem.* **1998**, *273*, 32753–32762. [[CrossRef](#)]
38. Spiegelhauer, O.; Dickert, F.; Mende, S.; Niks, D.; Hille, R.; Ullmann, M.; Dobbek, H. Kinetic characterization of xenobiotic reductase a from *Pseudomonas putida* 86. *Biochemistry* **2009**, *48*, 11412–11420. [[CrossRef](#)]
39. Scholtissek, A.; Tischler, D.; Westphal, A.; van Berkel, W.; Paul, C. Old yellow enzyme-catalysed asymmetric hydrogenation: Linking family roots with improved catalysis. *Catalysts* **2017**, *7*, 130. [[CrossRef](#)]
40. Hummel, W.; Gröger, H. Strategies for regeneration of nicotinamide coenzymes emphasizing self-sufficient closed-loop recycling systems. *J. Biotechnol.* **2014**, *191*, 22–31. [[CrossRef](#)]
41. Knaus, T.; Paul, C.E.; Levy, C.W.; de Vries, S.; Mutti, F.G.; Hollmann, F.; Scrutton, N.S. Better than nature: Nicotinamide biomimetics that outperform natural coenzymes. *J. Am. Chem. Soc.* **2016**, *138*, 1033–1039. [[CrossRef](#)]
42. Lee, S.H.; Choi, D.S.; Pesic, M.; Lee, Y.W.; Paul, C.E.; Hollmann, F.; Park, C.B. Cofactor-free, direct photoactivation of enoate reductases for the asymmetric reduction of c=c bonds. *Angew. Chem. Int. Ed.* **2017**, *56*, 8681–8685. [[CrossRef](#)]
43. Litthauer, S.; Gargiulo, S.; van Heerden, E.; Hollmann, F.; Opperman, D.J. Heterologous expression and characterization of the ene-reductases from *Deinococcus radiodurans* and *Ralstonia metallidurans*. *J. Mol. Catal. B Enzym.* **2014**, *99*, 89–95. [[CrossRef](#)]
44. Davies, M.T. A universal buffer solution for use in ultra-violet spectrophotometry. *Analyst* **1959**, *84*, 248–251. [[CrossRef](#)]
45. Peters, C.; Kölsch, R.; Kadow, M.; Skalden, L.; Rudroff, F.; Mihovilovic, M.D.; Bornscheuer, U.T. Identification, characterization, and application of three enoate reductases from *Pseudomonas putida* in in vitro enzyme cascade reactions. *ChemCatChem* **2014**, *6*, 1021–1027. [[CrossRef](#)]
46. Pesic, M.; Fernández-Fueyo, E.; Hollmann, F. Characterization of the old yellow enzyme homolog from *Bacillus subtilis* (yqjm). *ChemistrySelect* **2017**, *2*, 3866–3871. [[CrossRef](#)]
47. Xu, M.-Y.; Pei, X.-Q.; Wu, Z.-L. Identification and characterization of a novel “thermophilic-like” old yellow enzyme from the genome of *Chryseobacterium* sp. Ca49. *J. Mol. Catal. B Enzym.* **2014**, *108*, 64–71. [[CrossRef](#)]
48. Zheng, L.; Lin, J.; Zhang, B.; Kuang, Y.; Wei, D. Identification of a yeast old yellow enzyme for highly enantioselective reduction of citral isomers to (R)-citronellal. *Bioresour. Bioprocess.* **2018**, *5*, 1–12. [[CrossRef](#)]
49. Rudroff, F.; Mihovilovic, M.D.; Gröger, H.; Snajdrova, R.; Iding, H.; Bornscheuer, U.T. Opportunities and challenges for combining chemo- and biocatalysis. *Nat. Catal.* **2018**, *1*, 12–22. [[CrossRef](#)]
50. Fryszkowska, A.; Toogood, H.; Sakuma, M.; Gardiner, J.M.; Stephens, G.M.; Scrutton, N.S. Asymmetric reduction of activated alkenes by pentaerythritol tetranitrate reductase: Specificity and control of stereochemical outcome by reaction optimisation. *Adv. Synth. Catal.* **2009**, *351*, 2976–2990. [[CrossRef](#)]
51. Tischler, D.; Gadke, E.; Eggerichs, D.; Gomez Baraibar, A.; Mugge, C.; Scholtissek, A.; Paul, C.E. Asymmetric reduction of (r)-carvone through a thermostable and organic-solvent-tolerant ene-reductase. *Chembiochem* **2019**. [[CrossRef](#)]
52. Robescu, M.S.; Niero, M.; Hall, M.; Cendron, L.; Bergantino, E. Two new ene-reductases from photosynthetic extremophiles enlarge the panel of old yellow enzymes: Ctoye and gsoye. *Appl. Microbiol. Biotechnol.* **2020**, *104*, 2051–2066. [[CrossRef](#)]
53. Riedel, A.; Mehnert, M.; Paul, C.E.; Westphal, A.H.; van Berkel, W.J.; Tischler, D. Functional characterization and stability improvement of a ‘thermophilic-like’ ene-reductase from *Rhodococcus opacus* 1cp. *Front. Microbiol.* **2015**, *6*, 1073. [[CrossRef](#)] [[PubMed](#)]
54. Hall, M.; Stueckler, C.; Ehammer, H.; Pointner, E.; Oberdorfer, G.; Gruber, K.; Hauer, B.; Stuermer, R.; Kroutil, W.; Macheroux, P.; et al. Asymmetric bioreduction of c=c bonds using enoate reductases opr1, opr3 and yqjm: Enzyme-based stereocontrol. *Adv. Synth. Catal.* **2008**, *350*, 411–418. [[CrossRef](#)]

55. Josuran, R. Prot pi. Available online: <https://www.protpi.ch/> (accessed on 22 January 2020).
56. Forneris, F.; Orru, R.; Bonivento, D.; Chiarelli, L.R.; Mattevi, A. Thermofad, a thermofluor-adapted flavin ad hoc detection system for protein folding and ligand binding. *FEBS J.* **2009**, *276*, 2833–2840. [[CrossRef](#)] [[PubMed](#)]



© 2020 by the authors. Licensee MDPI, Basel, Switzerland. This article is an open access article distributed under the terms and conditions of the Creative Commons Attribution (CC BY) license (<http://creativecommons.org/licenses/by/4.0/>).